Index

Figure S1. Original C4D oscillator circuit modifications. 2

Figure S2. Schematic shield UNO board. 3

Figure S3. Pneumatic schematic diagram. 4

Figure S4. Schematic diagram of the complete device 5

Table S1. 3D-printable STL files. 7

Table S2. Ion concentrations in working solutions. 8

Analysis of migration times using PeakMaster, along with measurements of both FWHM and the peak asymmetry factor for each ion. 9

Table S3. PeakMaster simulation of the analytes of Section 5.2 in the BGE (2.3 M HAc). 9

Table S4. Experimental apparent mobilities and PeakMaster effective mobilities of the analytes in 2.3 M HAc, together with the mobilities relative to K^+. 10

Table S5: Peak asymmetry of the analytes of Section 5.2 at the three concentration levels, and the corresponding EMD × c values. 11

Figure S5. Peak asymmetry of the analytes in Section 5.2. 12

Figure S6. Spatial variance budget of the peaks of Section 5.2. 13

Table S6: Spatial variance budget of the peaks of Section 5.2 at the three concentration levels. 13

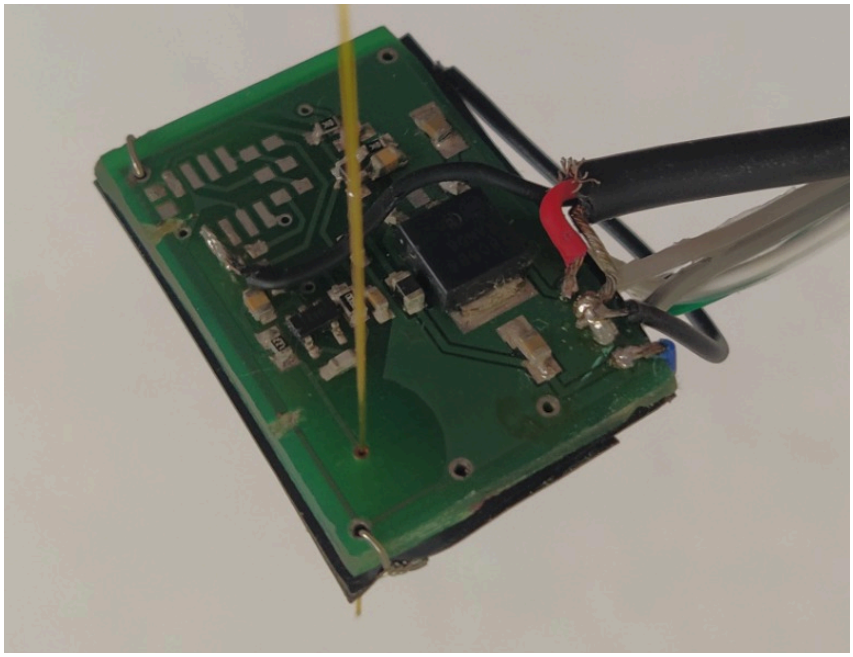
Table S7. Ion concentrations. 15

Table S8. SNR Analysis. 16

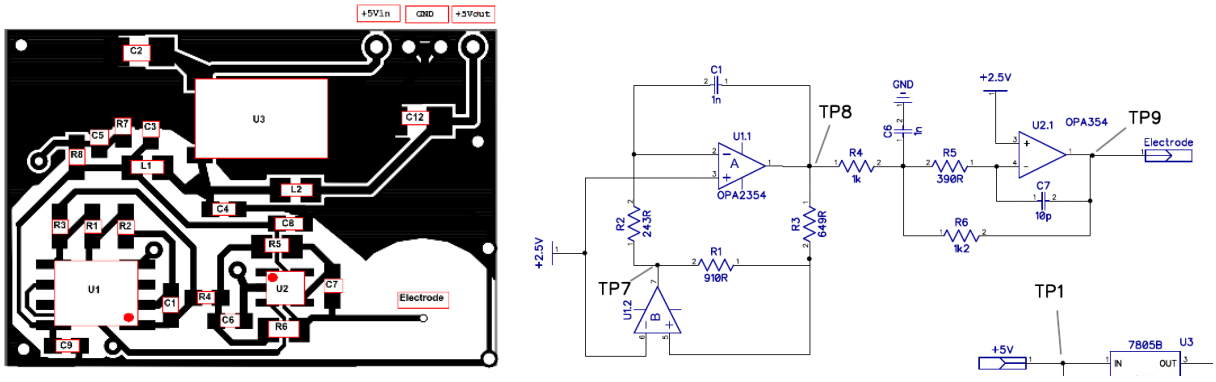
Table S9. Hydroponic nutrient concentrations. 17

Table S10. Reference method results for selected analytes. 18

Figure S1. Original C4D oscillator circuit modifications.

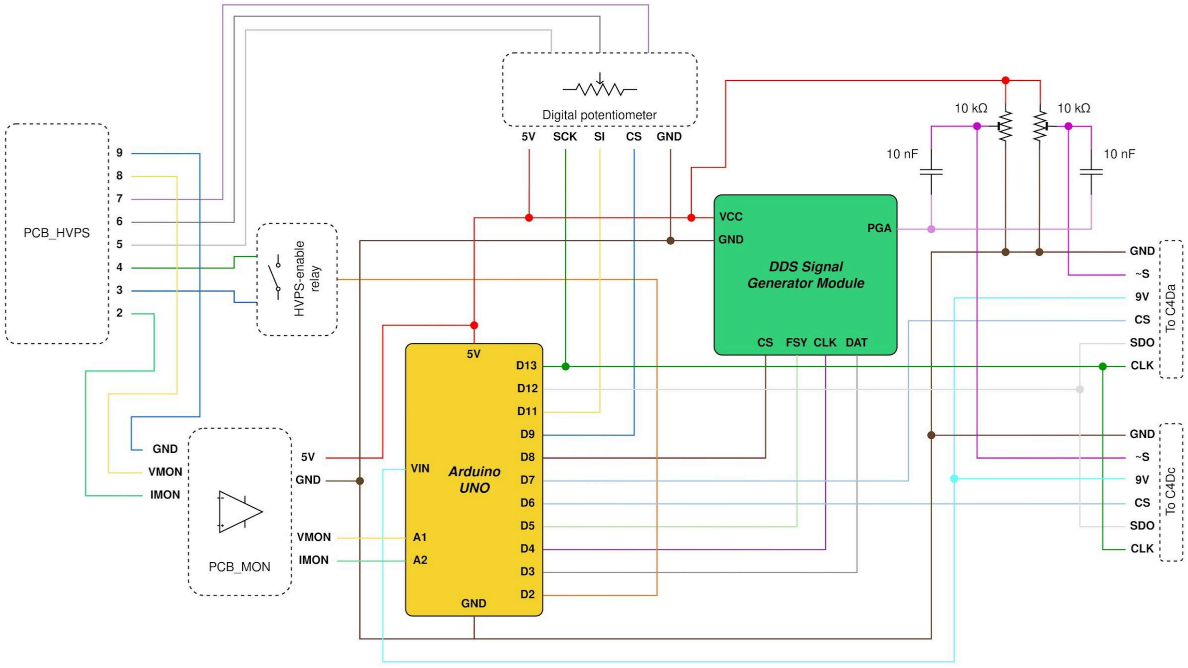


The original oscillator components responsible for generating the excitation waveform (U1, C1, C9, R1, R2, and R3) were not populated, while the final amplification stage connected to the detector electrode was retained (U2, C6, C7, R4, R5, R6). The excitation signal was instead supplied externally through an additional wire soldered to the T8 test point using the U1 pin 1 pad.



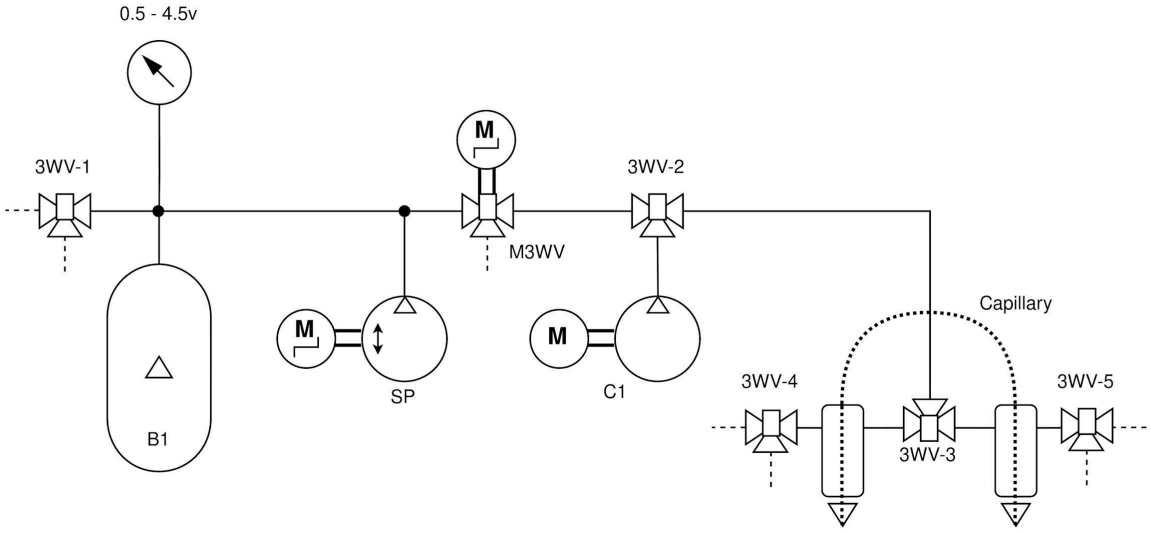
From https://github.com/claudimir-lago/openC4D

Figure S2. Schematic shield UNO board.



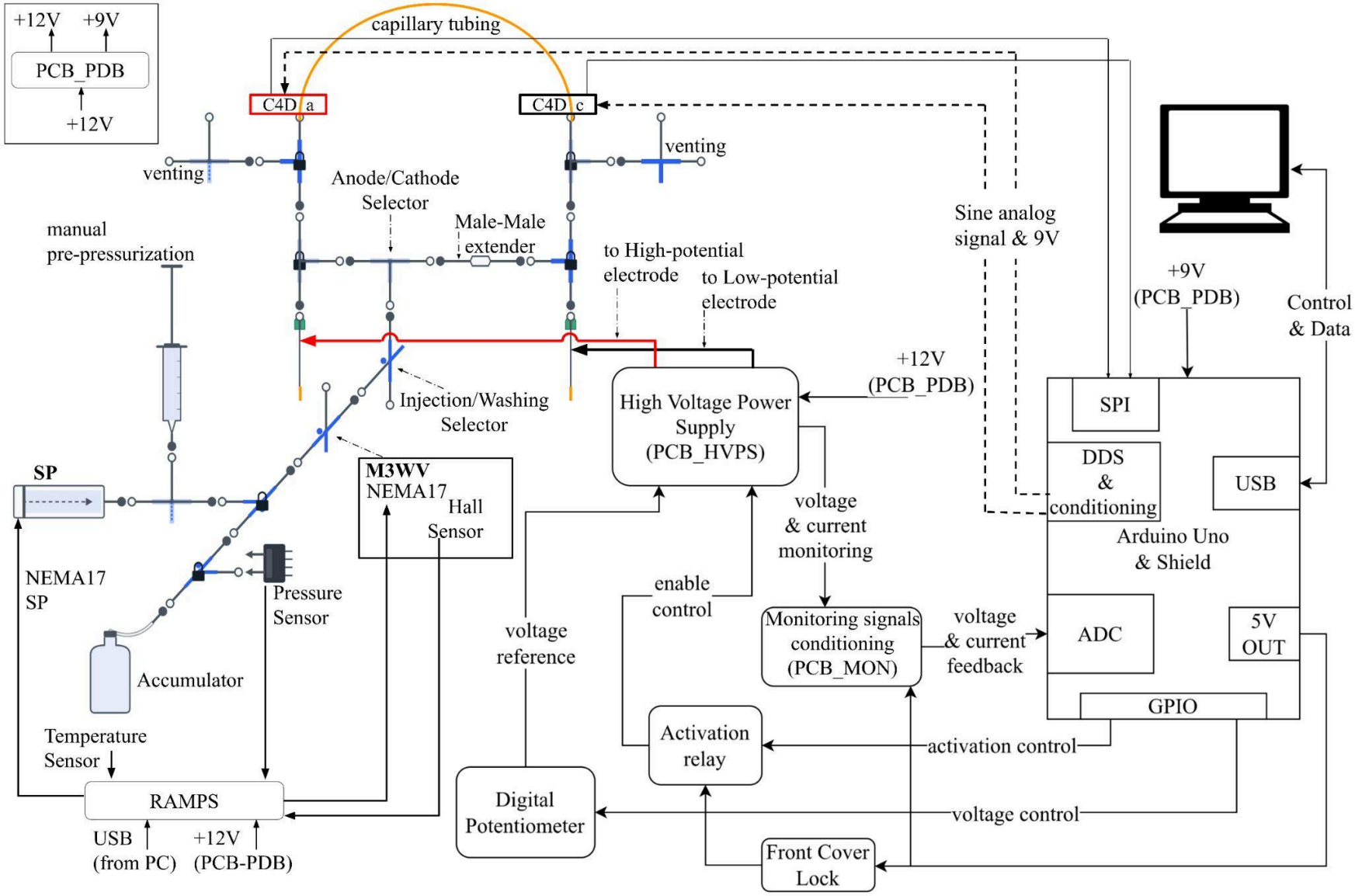
Circuit schematic for the custom Arduino UNO shield.

Figure S3. Pneumatic schematic diagram.



Pneumatic injection and flushing circuit. From left to right, the circuit comprises a low-pressure side, where the accumulator bottle (**B1**), NXP MPX5010DP differential pressure sensor (0–1.45 psi differential pressure), and syringe pump (**SP**) are interconnected and connected to the motorized three-way valve (**M3WV**). An additional three-way valve (**3WV-1**) provides a convenient Luer-standard access port for connection of a syringe or other compatible component, such as to manually pre-pressurize the line and minimize SP workload and displacement. The **M3WV** regulates the transfer of accumulated low-pressure air toward the downstream circuit. On the high-pressure side, a manually operated three-way valve (**3WV-2**) connects the circuit to the external mini-compressor (**C1**), providing the pressure source required for capillary flushing. The downstream three-way valve (**3WV-3**) routes the pressurized air toward the selected capillary end for injection or flushing, enabling access to either side of the capillary. Finally, **3WV-4** and **3WV-5** provide local venting paths to the atmosphere for pressure release at the respective capillary ends.

Figure S4. Schematic diagram of the complete device.



C4Da: C4D anode; C4Dc: C4D cathode
3WVs: components labeled with a padlock symbol denote valves whose positions must remain fixed during operation (acting as pneumatic tees). Blue lever indicators point toward the front plane, whereas lighter-shaded indicators point toward the rear plane.
Geometric projections and rotations are applied to represent 3D orientations schematically.
Luer connections: male Luer ports are indicated by filled circles and female Luer ports by empty circles.

Table S1. 3D-printable STL files.

Design File Name	File Type	Description
HEM-MountingBracket-A	3D mesh file (stl)	HEM Mating clamping block
HEM-MountingBracket-B	3D mesh file (stl)	HEM Key-retaining block
HEM-Spacer	3D mesh file (stl)	HEM Spacer
HEM-LowerInterfaceBlock	3D mesh file (stl)	HEM Lower Interface Block
VialHolder	3D mesh file (stl)	Vial Holder
M3WV-RotaryCoupler	3D mesh file (stl)	M3WV Rotary Coupler
M3WV-MountingSupport	3D mesh file (stl)	M3WV Mounting Support
M3WV-FrameMountingBracket	3D mesh file (stl)	M3WV Frame Mounting Bracket
C4DCase-A	3D mesh file (stl)	C4D Case A
C4DCase-B	3D mesh file (stl)	C4D Case B
C4DCaseFemaleLuerCapBracket	3D mesh file (stl)	C4D Case Female Luer Cap Bracket
CustomC4DMount-Left	3D mesh file (stl)	Custom C4D Mount Left
CustomC4DMount-Right	3D mesh file (stl)	Custom C4D Mount Right
EnclosureFixedGuideChannel	3D mesh file (stl)	Enclosure Fixed Guide Channel
EnclosureSlidingGuideChannel	3D mesh file (stl)	Enclosure Sliding Guide Channel
EnclosureFoot	3D mesh file (stl)	Enclosure Foot
CompressorCase	3D mesh file (stl)	Compressor Case
UNO-ControlUnitMountingBracket	3D mesh file (stl)	UNO Control Unit Mounting Bracket
PCB_PDBverticalHolder	3D mesh file (stl)	PCB_PDB Vertical Holder

Table S2. Ion concentrations in working solutions.

Ion	Stock concentration [mg·L^{-1}]	Dilution K10 115/10000 [mg·L^{-1}]	Dilution K20 225/10000 [mg·L^{-1}]	Dilution K30 345/10000 [mg·L^{-1}]
K^+	887.13	10.20	19.96	30.61
NO_3^-	1406.87	16.18	31.65	48.54
Ca^{2+}	311.00	3.58	7.00	10.73
HPO_4^{2-}	1489.56	17.13	33.52	51.39
Mg^{2+}	294.78	3.39	6.63	10.17
SO_4^{2-}	1165.28	13.40	26.22	40.20

Stock solutions were aqueous, and dilutions were prepared in 2.3 M HAc. Dilution ratios represent the volume (in μL) of stock solution diluted to a final volume of 10000 μL with 2.3 M HAc.

Analysis of migration times using PeakMaster, along with measurements of both FWHM and the peak asymmetry factor for each ion.

To compare the experimental results with theory, the effective mobilities of the analytes in the BGE (2.3 M HAc, pH 2.20, ionic strength 6.9 mM) were simulated with PeakMaster, with ionic-strength correction and the experimental geometry and voltage (L_tot = 50 cm, L_det = 13 cm, 8 kV). Results are shown in Table S3:

Table S3. PeakMaster simulation of the analytes of Section 5.2 in the BGE (2.3 M HAc).

Constituent	Ion	Detector	u_eff [a]	t_max (min)	t_max (s)	EMD [b]	Limiting mobilities [a]	pKa
Potassium	K^+	C4Dc	73.574	1.817	109.0	8.131	u(+1) = 76.2	13.0
Calcium	Ca^{2+}	C4Dc	55.949	2.355	141.3	19.680	u(+2) = 61.7; u(+1) = 30.9	12.6; 13.6
Magnesium	Mg^{2+}	C4Dc	49.460	2.661	159.7	20.942	u(+2) = 55.0; u(+1) = 27.5	11.4; 12.2
Nitric acid	NO_3^-	C4Da	−70.117	1.985	119.1	−21.940	u(−1) = 74.1	−1.4
Sulfuric acid	SO_4^{2-} / HSO_4^-	C4Da	−66.601	2.121	127.3	−39.953	u(−2) = 82.9; u(−1) = 52.0	1.9; −3.0

[a] 10^{-9} m^2 V^{-1} s^{-1}.

[b] 10^{-3} S m^2 mol^{-1}.

Simulation conditions: BGE 2.3 M acetic acid (u(−1) = 42.4, pKa = 4.756); L_tot = 50 cm, L_det = 13 cm; 8 kV; no EOF;
ionic-strength correction applied. Calculated BGE properties: pH 2.198, ionic strength 6.905 mM, conductivity 0.262 S m^{-1},
buffer capacity 31.75 mM. Polarity at the injection site: negative for anions (C4Da), positive for cations (C4Dc).
t_max assumes full voltage from t = 0 and should be compared with experimental t_m − 5 s (10 s linear ramp).

Phosphate was not included because it migrates too slowly to be detected within the analysis time. Experimental apparent mobilities were calculated from the apex migration times, corrected for the 10 s linear voltage ramp (t_eff = t_m − 5 s). The absolute experimental mobilities were lower than the predicted values by a nearly constant factor (μ_exp/μ_PM = 0.70–0.71 for K^+, Ca^{2+}, Mg^{2+} and NO_3^-). Because this factor is common to all ions, it does not affect the migration order or the relative spacing of the peaks. Its most likely causes are the higher viscosity of 2.3 M HAc compared with water and the difference between the operating temperature (20 °C) and the 25 °C reference of the PeakMaster database. To remove this common factor, the mobility of each ion was normalized to that of K^+ within each run and then averaged over the nine runs (Table S4). The experimental relative mobilities agreed with the predicted values to within 2 % for Ca^{2+} (0.759 ± 0.002 vs. 0.760; −0.2 %), Mg^{2+} (0.683 ± 0.002 vs. 0.672; +1.6 %) and NO_3^- (0.952 ± 0.018 vs. 0.953; −0.2 %). Sulfate was the only exception: its relative mobility (0.805 ± 0.015) was 11 % lower than predicted (0.905). Sulfate is the only analyte in this set whose

effective mobility depends on an acid–base equilibrium close to the pH of the BGE (pKa of HSO_4^- ≈ 1.9 vs. pH 2.2), so its degree of protonation, and therefore its effective charge, is very sensitive to small shifts in pKa or pH. The lower permittivity of the ~14 % (w/w) acetic acid medium may raise this pKa, increasing protonation and reducing the effective mobility relative to the aqueous-based prediction. Overall, the device separates the analytes in the order and with the relative spacing predicted from their effective mobilities, which implicitly account for charge, size and ionic strength.

Table S4. Experimental apparent mobilities and PeakMaster effective mobilities of the analytes in 2.3 M HAc, together with the mobilities relative to K^+.

Ion	z	μ_exp [a]	μ_PM [b]	μ_exp/μ_PM	μ_rel, exp [c]	μ_rel, PM	Δ (%) [d]
K^+	1	51.57 ± 0.71	73.57	0.701	1	1	—
Ca^{2+}	2	39.13 ± 0.61	55.95	0.699	0.7588 ± 0.0023	0.760	−0.2
Mg^{2+}	2	35.22 ± 0.57	49.46	0.712	0.6830 ± 0.0019	0.672	1.6
NO_3^-	−1	−49.06 ± 0.27	−70.12	0.700	0.9516 ± 0.0178	0.953	−0.2
SO_4^{2-}	−2	−41.52 ± 0.26	−66.60	0.623	0.8054 ± 0.0152	0.905	−11.0

Mobilities in 10^{-9} m^2 V^{-1} s^{-1}.

[a] Mean ± SD of nine runs (K10, K20 and K30, n = 3 each), calculated from apex migration times corrected for the 10 s voltage ramp (t_eff = t_m − 5 s), with L_det = 13 cm, L_tot = 50 cm and V = 8 kV.

[b] PeakMaster effective mobility with ionic-strength correction (BGE: 2.3 M HAc, pH 2.20, I = 6.9 mM).

[c] |μ_i/μ_K^+| calculated within each run and averaged over the nine runs (mean ± SD).

[d] Δ = (μ_rel, exp − μ_rel, PM)/μ_rel, PM × 100.

Asymmetry

Peak asymmetry was evaluated with the asymmetry factor at 10 % of peak height (A_s = b/a; A_s > 1 indicates tailing and A_s < 1 fronting). All cation peaks showed tailing and all anion peaks showed fronting, and the asymmetry increased systematically with sample concentration: from K10 to K30, A_s rose from 1.1–1.8 to 2.4–3.6 for the cations and decreased from 0.31–0.41 to 0.18–0.20 for the anions (Table S5). This behavior is characteristic of electromigration dispersion (EMD), which arises when the conductivity of the analyte zone differs from that of the BGE and is particularly pronounced at the low ionic strength of the BGE used here (6.9 mM). PeakMaster predicts positive EMD values (tailing) for the cations and negative values (fronting) for the anions (Table S3), in agreement with the sign of the asymmetry in all 45 peaks analyzed. Because the magnitude of this distortion scales with the product of the EMD coefficient and the analyte concentration, ln A_s was compared with EMD × c (Figure S5). For the cations, ln A_s correlated with EMD × c (r = 0.89, n = 27) much better than with concentration alone (r = 0.49), and the regression line passed close to the origin

(intercept 0.06), so the three cations fell approximately on a common line. Mg^{2+}, which has the largest EMD × c, was the most asymmetric cation at all three concentration levels, whereas the predicted order of K^{+} and Ca^{2+} was reproduced only at the lowest level. For the anions, PeakMaster predicts nearly identical EMD × c values for NO_3^- and SO_4^{2-} at each concentration level, and both showed similar A_s values that decreased together with concentration (r = 0.86, n = 18). Their fronting, however, was stronger than a simple proportional relationship would predict (intercept −0.64), which may be partly due to the baseline step that follows the NO_3^- peak in the anion channel and affects the 10 % crossing, and partly to the nonlinear dependence of A_s on EMD × c as peaks approach a triangular shape. Overall, peak asymmetry is governed by the electromigration properties of each analyte in the BGE and by its concentration, rather than by instrumental band broadening, which would be expected to distort the peaks of both channels in the same direction.

Table S5: Peak asymmetry of the analytes of Section 5.2 at the three concentration levels, and the corresponding EMD × c values.

Ion	Level	c (mM) [a]	EMD [b]	EMD × c [c]	A_s (10 %) [d]	ln A_s
K^{+}	K10	0.261	8.131	2.120	1.54 ± 0.26	0.42
	K20	0.511		4.150	1.84 ± 0.20	0.600
	K30	0.783		6.370	2.45 ± 0.03	0.890
Ca^{2+}	K10	0.089	19.68	1.760	1.12 ± 0.08	0.110
	K20	0.175		3.440	1.86 ± 0.16	0.620
	K30	0.268		5.27	2.67 ± 0.09	0.98
Mg^{2+}	K10	0.139	20.942	2.92	1.79 ± 0.49	0.55
	K20	0.273		5.71	2.12 ± 0.12	0.75
	K30	0.418		8.76	3.57 ± 0.20	1.27
NO_3^-	K10	0.261	−21.940	−5.73	0.31 ± 0.02	−1.16
	K20	0.51		−11.20	0.27 ± 0.02	−1.31
	K30	0.783		−17.18	0.18 ± 0.02	−1.70
SO_4^{2-}	K10	0.14	−39.953	−5.57	0.41 ± 0.01	−0.89
	K20	0.273		−10.91	0.38 ± 0.04	−0.99
	K30	0.419		−16.72	0.20 ± 0.01	−1.62

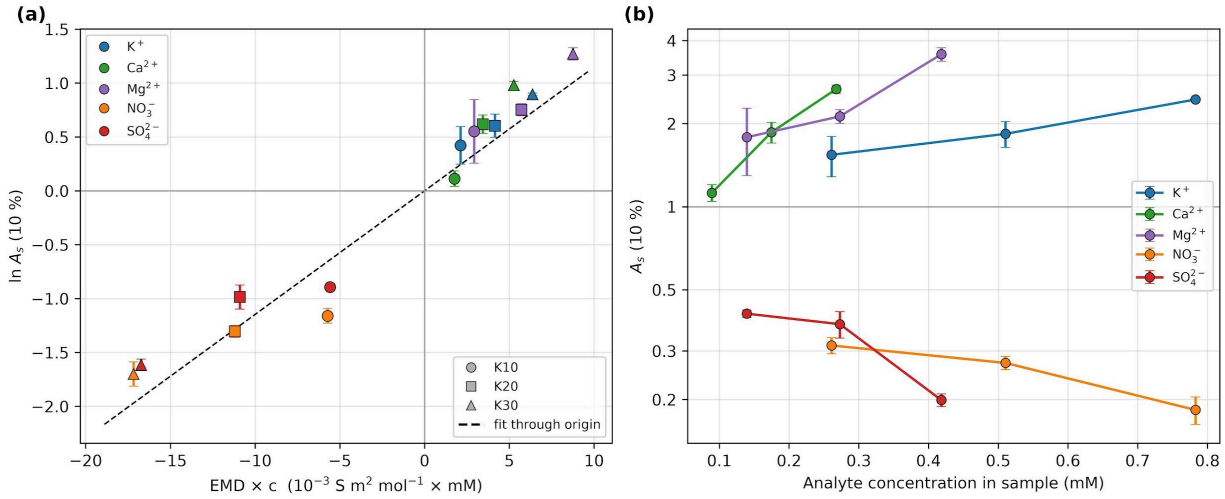
[a] Analyte concentration in the injected sample, calculated from Table S2.

[b] Electromigration dispersion coefficient calculated with PeakMaster (10^{-3} S m² mol^{-1}; Table S3).

[c] 10^{-3} S m² mol^{-1} × mM.

[d] Asymmetry factor at 10 % of peak height (A_s = b/a), mean ± SD (n = 3). A_s > 1: tailing; A_s < 1: fronting.

Figure S5. Peak asymmetry of the analytes in Section 5.2.



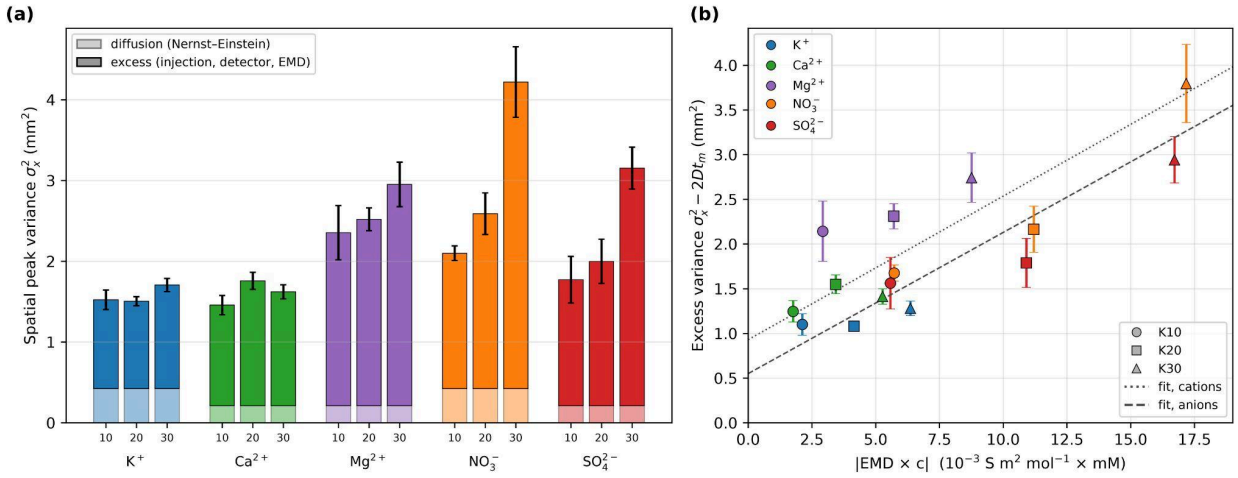
(a) ln A_s (10 %) vs. EMD × c, where EMD is the electromigration dispersion coefficient calculated with PeakMaster (Table S3) and c the analyte concentration in the injected sample (Table S2). Colors indicate the ion and symbols the concentration level (K10, K20, K30). The points are means ± SD (n = 3), and the dashed line is a least-squares fit through the origin to the individual runs (n = 45).
(b) A_s (10 %) vs. analyte concentration (logarithmic scale). The horizontal line at A_s = 1 corresponds to a symmetric peak.

FWHM

Because the temporal peak width depends on the migration velocity, slower ions give broader peaks in time even when their spatial width is the same. The FWHM values (3.5–7.1 s) were therefore converted into spatial standard deviations at the detector, σ_x = (FWHM/2.355)·v, where v = L_det/(t_m − 5 s), and a variance budget was established for each peak (Figure S6, Table S6). The contribution of longitudinal diffusion was calculated as σ²_diff = 2Dt_m, with D obtained from the experimental mobility through the Nernst–Einstein relation, D = |μ|kT/(|z|e), so that the viscosity and temperature of the BGE are implicitly included. This is the only band-broadening term in which the charge-to-size ratio of the ion enters directly. In a diffusion-limited separation, the plate number is N_diff = |z|eEL_det/(2kT): because both mobility and diffusion coefficient scale inversely with ion size, size cancels and only the charge remains, giving N_diff ≈ 41,200 for monovalent and 82,300 for divalent ions under our conditions. The experimental plate numbers (4,300–12,200) were well below these limits, and diffusion accounted for only 25–28 % of the spatial peak variance for K^+, 10–20 % for NO_3^- and 7–14 % for the divalent ions. Peak width is therefore not controlled by the charge-to-size ratio of the analytes. Most of the variance came from an excess term comprising the injection plug, the detector length and EMD. For the anions, this excess variance increased linearly with |EMD × c| (r = 0.87, n = 18), the widest peak being NO_3^- at the highest concentration level. For K^+ and Ca^{2+}, which have low EMD × c values, the excess variance remained nearly constant (1.1–1.5 mm²), and the slope for the cations was similar to that of the anions (0.16 mm² per unit of EMD × c). Mg^{2+} showed about 1 mm² more excess variance than expected from its EMD × c at all

three levels, which was not explained by this analysis. Extrapolation to zero EMD × c gave an excess variance of 0.55–0.93 mm², equivalent to a rectangular zone of ~2.6–3.3 mm, which represents the combined contribution of the injection plug and the detector at each capillary end. Because σ_x was derived from the FWHM assuming a Gaussian profile, these values are approximate, particularly for the most asymmetric peaks.

Figure S6. Spatial variance budget of the peaks of Section 5.2.



(a) Spatial peak variance σ_x² for each ion and concentration level (10, 20 and 30 correspond to K10, K20 and K30), calculated from the FWHM and the migration velocity. Light segments: longitudinal-diffusion contribution (2Dt_m, with D from the Nernst–Einstein relation and the experimental mobility). Dark segments: excess variance. Error bars: SD of σ_x² (n = 3). (b) Excess variance (σ_x² − 2Dt_m) vs. |EMD × c|. Colors indicate the ion and symbols the concentration level; the points are means ± SD (n = 3). The lines are least-squares fits to the individual runs of the cations (dotted, n = 27) and the anions (dashed, n = 18).

Table S6: Spatial variance budget of the peaks of Section 5.2 at the three concentration levels.

Ion	Level	FWHM (s) [a]	FWHM/t_eff (%) [b]	D [c]	σ_x² [d]	σ²_diff [e]	σ²_excess [f]	Diffusion (%) [g]	N_exp [h]	N_diff [i]	EMD × c [j]
K^+	K10	3.58 ± 0.13	2.23	1.280	1.52	0.42	1.1	28	11,800	41,200	2.12
	K20	3.48 ± 0.07	2.22	1.310	1.51	0.420	1.08	28	12,000		4.15
	K30	3.68 ± 0.09	2.36	1.320	1.71	0.420	1.28	25	10,600		6.37
Ca^{2+}	K10	4.63 ± 0.17	2.18	0.480	1.46	0.210	1.25	14	12,200	82,300	1.76
	K20	4.93 ±	2.4	0.500	1.76	0.210	1.55	12	10,100		3.44

		0.15									
	K30	4.74 ± 0.12	2.31	0.5	1.62	0.21	1.41	13	10,900		5.27
Mg^{2+}	K10	6.54 ± 0.46	2.77	0.44	2.35	0.21	2.14	9	7,600	82,300	2.92
	K20	6.57 ± 0.18	2.87	0.45	2.52	0.21	2.31	8	7,000		5.71
	K30	7.08 ± 0.32	3.11	0.45	2.95	0.21	2.74	7	6,000		8.76
NO_3^-	K10	4.32 ± 0.10	2.62	1.25	2.1	0.42	1.68	20	8,600	41,200	−5.73
	K20	4.82 ± 0.23	2.91	1.24	2.59	0.42	2.17	16	7,000		−11.20
	K30	6.20 ± 0.34	3.72	1.23	4.22	0.42	3.8	10	4,300		−17.18
SO_4^{2-}	K10	4.68 ± 0.38	2.41	0.53	1.77	0.21	1.56	12	10,200	82,300	−5.57
	K20	4.99 ± 0.35	2.56	0.53	2	0.21	1.79	11	9,000		−10.91
	K30	6.34 ± 0.27	3.21	0.52	3.15	0.21	2.94	7	5,700		−16.72

All values are means of three runs (n = 3).

[a] Full width at half maximum, mean ± SD.

[b] Relative peak width, with t_eff = t_m − 5 s (10 s linear voltage ramp).

[c] Diffusion coefficient (10^{-9} m^2 s^{-1}) from the Nernst–Einstein relation, D = |μ|kT/(|z|e), using the experimental apparent mobility and T = 293 K. Nominal charges were used (|z| = 2 for sulfate).

[d] Spatial peak variance at the detector (mm^2), σ_x = (FWHM/2.355)·L_det/t_eff, assuming a Gaussian profile.

[e] Longitudinal-diffusion variance (mm^2), σ²_diff = 2Dt_m.

[f] Excess variance (mm^2), σ_x² − σ²_diff, attributed to the injection plug, the detector length and electromigration dispersion.

[g] Fraction of σ_x² due to diffusion.

[h] Experimental plate number.

[i] Diffusion-limited plate number, N_diff = |z|eEL_det/(2kT), with E = V/L_tot. It depends only on the ion charge.

[j] 10^{-3} S m^2 mol^{-1} × mM (Table S5).

Table S7. Ion concentrations.

Ion	Concentration [mg·L^{-1}]
K^+	17.40
NO_3^-	27.60
Ca^{2+}	13.44
Cl^-	23.78
Mg^{2+}	6.59
SO_4^{2-}	26.07

The reported concentrations were obtained by diluting stock solutions with 2.3 M HAc.

Table S8. SNR Analysis.

Ion	Frequency [kHz]	Lower limit [s]	Time max signal [s]	Upper limit [s]	Height (H) [a.u.]	Noise RMS [a.u.]	SNR= H/(RMS)
Cl^-	1000	164.67	176.80	178.89	3314.09	187.70	17.66º
	800	163.00	177.80	180.26	2762.92	60.21	45.89
	600	162.47	176.77	179.23	1816.51	99.27	18.30
NO_3^-	1000	176.31	185.89	188.29	3421.23	187.70	18.23
	800	175.47	187.21	189.47	3353.40	60.21	55.69
	600	175.33	186.01	188.35	2227.65	99.27	22.44
SO_4^{2-}	1000	207.40	220.22	222.98	2980.58	187.70	15.88
	800	208.03	222.28	224.78	2960.08	60.21	49.16
	600	207.50	220.87	223.31	1868.92	99.27	18.83
K^+	1000	156.17	158.86	164.02	1910.35	151.25	12.63
	800	157.46	160.23	164.84	1267.54	63.88	19.84
	600	158.52	161.17	165.31	766.18	98.41	7.79
Ca^{2+}	1000	202.23	204.30	211.83	3294.07	151.25	21.78
	800	204.02	206.40	212.86	2178.11	63.88	34.10
	600	205.45	208.02	213.98	1302.66	98.41	13.24
Mg^{2+}	1000	223.28	226.72	235.71	2346.95	151.25	15.52
	800	224.81	229.38	237.01	1609.23	63.88	25.19
	600	226.57	231.37	238.03	968.23	98.41	9.84

Table S9. Hydroponic nutrient concentrations.

Ion	Declared concentration [mg·L^{-1}]	Dilution in HAc [mg·L^{-1}]
K^+	50000.00	18.75
Mg^{2+}	8000.00	3.00
NO_3^- *	132878.57	49.83
SO_4^{2-} **	78048.75	29.27
* The sample declares 3% total N, here expressed as NO_3^-		
** The sample declares 2.6% S from Sulphate, here expressed as SO_4^{2-}		

Table S10. Reference method results for selected analytes.

Ion	Analytical Technique	Concentration ($mg \cdot L^{-1}$)
Calcium	AAS - Standard Methods 3500-Ca.B	< 0.50
Magnesium	AAS - Standard Methods 3500-Mg.B	7631.60
Sodium	AAS - Standard Methods 3500-Na.B	4563.60
Potassium	AAS - Standard Methods 3500-K.B	45714.30
Ammonium	Colorimetry - Standard Methods 4500-NH_3.D	190.00
Nitrate	Colorimetry - Standard Methods 4500-NO_3^-	83500.00
Nitrite	Colorimetry - Standard Methods 4500-NO_2^-.B	< 0.02
Chloride	Colorimetry - Standard Methods 4500-Cl^-.B	4.00
Sulfate	Turbidimetry - Standard Methods 4500-SO_4^{2-}.E	81000.00